Response of the ATLAS tile calorimeter prototype to muons

Ziad Zj Ajaltouni, F. Albiol, A. Alifanov, P. Amaral, A. Amorim, K.J. Anderson, C. Angelini, A. Astvatsaturov, D. Autiero, F. Badaud, et al.

EUROPEAN ORGANIZATION FOR NUCLEAR RESEARCH

CERN-PPE/96-173
December 13, 1996

Response of the ATLAS Tile Calorimeter Prototype to Muons

Z. Ajaltouni[e], F. Albiol[r], A. Alifanov[k], P. Amaral[i1,i2], A. Amorim[i1,i2], K. Anderson[c], C. Angelini[l], A. Astvatsaturov[g], D. Autiero[l], F. Badaud[e], G. Barreira[i1], S. Berglund[q], G. Blanchot[b], E. Blucher[c], C. Blaj[d], A. Bogush[k], C. Bohm[q], V. Boldea[d], O. Borisov[g], M. Bosman[b], N. Bouhemaid[e], P. Brette[e], C. Bromberg[j], M. Brossard[e], J. Budagov[g], L. Caloba[p], J. Carvalho[i3], P. Casado[b], M. Cavalli-Sforza[b], V. Cavasinni[l], R. Chadelas[e], J.-C. Chevaleyre[e], I. Chirikov-Zorin[g], G. Chlachidze[g], M. Cobal[f], F. Cogswell[h], F. Colaço[i4], S. Constantinescu[d], D. Costanzo[l], M. Crouau[e], F. Daudon[e], M. David[i1,i2], T. Davidek[m], J. Dawson[a], J.-J. Dugne[e], K. De[s], T. Del Prete[l], A. De Santo[l], B. Di Girolamo[l], S. Dita[d], J. Dolejsi[m], Z. Dolezal[m], R. Downing[h], I. Efthymiopoulos[b], D. Errede[h], S. Errede[h], H. Evans[c], A. Ferrer[r], V. Flaminio[l], E. Gallas[s], M. Gaspar[p], O. Gildemeister[f], V. Glagolev[g], V. Golubev[k], A. Gomes[i1,i2], V. Grabsky[t], M. Haney[h], H. Hakopian[t], S. Hellman[q], A. Henriques[i1], S. Holmgren[q], P.F. Honoré[r], J. Huston[j], Yu. Ivanyushenkov[b], E. Johansson[q], K. Jon-And[q], A. Juste[b], S. Kakurin[g], G. Karapetian[f], A. Karyukhin[o], Yu. Khokhlov[o], V. Klyukhin[o], V. Kolomoets[g], S. Kopikov[o], M. Kostrikov[o], V. Kovtun[g], V. Kukhtin[g], M. Kulagin[o], Y. Kulchitsky[k], S. Lami[l], V. Lapin[o], C. Lazzeroni[l], A. Lebedev[g], R. Leitner[m], J. Li[s], I. Liba[g], Yu. Lomakin[g], O. Lomakina[g], M. Lokajicek[n], A. Maio[i1,i2], S. Malyukov[g], F. Marroquin[p], J.P. Martins[i1,i2], E. Mazzoni[l], F. Merritt[c], B. Michel[e], R. Miller[j], I. Minashvili[g], Ll. Miralles[b], E. Mnatsakanian[t], G. Montarou[e], G.S. Muanza[e], S. Nemecek[n], M. Nessi[f], A. Onofre[i3,i4], S. Orteu[b], C. Padilla[b], D. Pallin[e], D. Pantea[g], J. Patriarca[i1], A. Pereira[p], J.A. Perlas[b], J. Pilcher[c], J. Pinhão[i3], L. Poggioli[f], S. Poirot[e], L. Price[a], Y. Protopopov[o], J. Proudfoot[a], O. Pukhov[g], G. Reinmuth[e], G. Renzoni[l], R. Richards[j], I. Riu[b], V. Romanov[g], B. Ronceux[b], V. Rumyantsev[k], N. Russakovich[g], H. Sanders[c], J. Santos[i1], L. Sawyer[s], L.-P. Says[e], J.M. Seixas[p], B. Sellden[q], A. Semenov[g], V. Senchishin[g], A. Shchelchkov[g], V. Shevtsov[g], M. Shochet[c], V. Sidorov[o], V. Simaitis[h], A. Sissakian[g], A. Solodkov[e], P. Sonderegger[f], K. Soustruznik[m], R. Stanek[a], E. Starchenko[o], R. Stephens[s], S. Studenov[g], M. Suk[m], A. Surkov[o], F. Tang[c], S. Tardell[q], P. Tas[m], F. Teubert[b], J. Thaler[h], S. Tokar[g], N. Topilin[g], Z. Trka[m], A. Turcot[c], M. Turcotte[s], S. Valkar[m], M.J. Varandas[i1,i2], A. Vartapetian[t], F. Vazeille[e], V. Vinogradov[g], S. Vorozhtsov[g], D. Wagner[c], A. White[s], H. Wolters[i4], N. Yamdagni[q], G. Yarygin[g], C. Yosef[j], A. Zaitsev[o], M. Zdrazil[m]

[a] *Argonne National Laboratory, USA*
[b] *Institut de Fisica d'Altes Energies, Universitat Autònoma de Barcelona, Spain*
[c] *University of Chicago, USA*
[d] *Institute of Atomic Physics, Bucharest, Rumania*
[e] *LPC Clermont–Ferrand, Université Blaise Pascal / CNRS–IN2P3, France*
[f] *CERN, Geneva, Switzerland*
[g] *JINR Dubna, Russia*
[h] *University of Illinois, USA*
[i] *1) LIP-Lisbon, 2) FCUL-Univ. of Lisbon, 3) LIP and FCTUC-Univ. of Coimbra, 4) Univ. Católica Figueira da Foz, Portugal*
[j] *Michigan State University, USA*
[k] *Institute of Physics ASB, Minsk, Belarus*
[l] *Pisa University and INFN, Pisa, Italy*
[m] *Charles University, Prague, Czech Republic*
[n] *Academy of Science, Prague, Czech Republic*
[o] *Institute for High Energy Physics, Protvino, Russia*
[p] *COPPE/EE/UFRJ, Rio de Janeiro, Brazil*
[q] *Stockohlm University, Sweden*
[r] *IFIC Valencia, Spain*
[s] *University of Texas at Arlington, USA*
[t] *Yerevan Physics Institute, Armenia*

Abstract

A study of high energy muons traversing the ATLAS hadron Tile calorimeter in the barrel region in the energy range between 10 and 300 GeV is presented. Both test beam experimental data and Monte Carlo simulations are given and show good agreement. The Tile calorimeter capability of detecting isolated muons over the above energy range is demonstrated. A signal to background ratio of about 10 is expected for the nominal LHC luminosity ($10^{34} cm^{-2} sec^{-1}$). The photoelectron statistics effect in the muon shape response is shown. The e/mip ratio is found to be 0.81 ± 0.03; the e/μ ratio is in the range 0.91 - 0.97.

The energy loss of a muon in the calorimeter, dominated by the energy lost in the absorber, can be correlated to the energy loss in the active material. This correlation allows one to correct on an event by event basis the muon energy loss in the calorimeter and therefore reduce the low energy tails in the muon momentum distribution.

1 Introduction

In the ATLAS detector muons with energies greater than 2 GeV will be measured with a system of chambers placed inside an air core toroid after crossing more than 100 radiation lengths of electromagnetic and hadronic calorimetry [1]. The muons will lose some fraction of their energy in the calorimeter material preceding the muon spectrometer. This fraction will fluctuate from event to event and therefore to achieve high precision on the muon momentum measurement it is important to measure this energy loss. Although the major goal of the ATLAS hadron calorimeter (Tile calorimeter) will be to identify particles and jets and to measure their energy and direction, as well as to measure the total missing transverse energy, it can also measure the muon energy loss. Since the signal produced by muons passing through a calorimeter is small compared to signals from hadron showers, the additional requirement to identify muons with the Tile calorimeter puts further constraint on the readout system. Low noise and high photoelectron statistics are additional important parameters to measure the energy deposited by muons.

The ATLAS Barrel calorimeter [1] will include a Pb-Liquid Argon (LAr) electromagnetic calorimeter with accordion-shaped electrodes, and a large scintillating Tile hadronic calorimeter, with iron as absorber material and scintillating plates read out by wavelength shifting fibres. The momentum resolution of the muon spectrometers in ATLAS are specified as $\Delta p_T/p_T = 2\%$ at 50 GeV and about 10% at 1000 GeV. The fluctuations of the energy loss from the absorber material in the calorimeter in front of the muon spectrometer will limit the precision of the muon momentum measurement for muon p_T below 100 GeV. In general these fluctuations are reduced when the calorimeter absorber is made out of a relatively low Z material, like iron, as it is the case for the ATLAS Tile calorimeter. In ATLAS the energy loss in the calorimeters will dominate the muon momentum resolution below 30 GeV. Above 30 GeV multiple scattering in the muon chambers and measurement errors will dominate as seen in Fig. 1 [1].

Identification of soft muons will be an important tool to tag b-jets. For example in searches for Higgs in the intermediate mass region through the decay H $\rightarrow b\bar{b}$ (with a typical transverse momentum of b-jet $p_T \sim 40$ GeV) or tagging t-quarks through the decay t$\rightarrow$ Wb (b-jet $p_T \sim 70$ GeV).

In the momentum range of 10 to 100 GeV, the correlation between the energy loss in the active and passive material of the Tile calorimeter (plastic scintillator tiles and iron, respectively) can be used to correct the measurement for the energy loss of a muon traversing the full calorimeter depth. This would allow us to improve the muon momentum measurement in the spectrometers or at least to reduce the tails in the muon momentum distribution. The capability to detect the Higgs boson in its intermediate mass range via the decay channel $H \rightarrow ZZ^* \rightarrow 4\mu$ could profit from such an improved muon momentum measurement.

These aspects were investigated with data obtained in a test beam at the

CERN-SPS. The experimental results have been compared with extensive Monte Carlo (MC) simulations.

The present paper is organized as follows. Section 2 describes the calorimeter prototype and the test beam setup. The test beam results are discussed in Section 3 and compared to our simulation. Results on the energy, angular and position dependence of the muon signals are given. The e/mip, μ/mip and the sampling fraction for electrons and muons are determined. We use the simulation results in Section 4 to show the accuracy on the muon energy loss measurement and the extent of tails in the muon momentum distribution in the ATLAS spectrometer when such energy loss corrections are applied on the event by event basis. Conclusions are given in Section 5.

2 Test Beam Setup

The data discussed in this paper were taken with a calorimeter prototype consisting of five modules, each spanning $2\pi/64$ in azimuth [1, 2, 3], with a front face of 100×20 cm^2. The longitudinal depth is 180 cm, corresponding to 8.9 interaction lengths (λ) at $\eta = 0$ or to 80.5 radiation lengths (X_0).

The Tile calorimeter uses iron as absorber and scintillator plates, read out by wavelength-shifting fibres, as the sampling material. An innovative feature of this design is the orientation of the tiles which are aligned parallel to the $\eta = 0$ plane and staggered in depth. Fibres running radially collect light from the tiles at both of their open edges. Readout cells are then defined by grouping together a set of fibres into a photomultiplier (PMT). Thus each calorimeter cell is read out by 2 PMTs. The calorimeter is radially segmented into four depth samplings (corresponding to 1.5, 2, 2.5 and 3 λ at η=0) and five transverse segments, thus providing for a projective geometry in azimuth, but not in polar angle. The gain of the PMT's was set to deliver $\simeq 6$ pC/GeV, where the digitized charge expressed in pC are always normalized by deposited energy for electrons at 10^o incident angle. The high voltage value of each PMT has been adjusted by running a radioactive source through each scintillating tile. The current induced in the PMT is proportional to the PMT gain and to the photoelectron yield of the calorimeter for the scintillation light induced by the source. A pulsed laser system, illuminating each PMT by means of clear fibres, was used to monitor the gains of the phototubes.

The five Tile calorimeter modules, stacked along the azimuthal (ϕ) direction, were mounted on a scanning table allowing precise scans of the impact point on the calorimeter front face z, and of the angles θ and ϕ of the beam to the axis of each module. See Fig. 2 .

Beam chambers and beam defining counters were placed upstream of the scanning table. Two scintillator walls with surface areas of about 1 m^2 were mounted on one side and at the back of the calorimeter to tag the lateral and

longitudinal leakage of hadronic showers. Data were taken with momentum-selected muons from 10 to 300 GeV/c incident on the calorimeter at polar angles between 0^o and 90^o.

A detailed simulation code of the calorimeter prototypes, based on GEANT 3.21, was produced and extensively tested. Besides giving a precise description of the geometry of the detector, the code simulates all known instrumental effects such as PMT noise, tile attenuation and nonuniformity, fibre attenuation and photoelectron statistics. To optimize comparison to the experimental data, the MC events were generated with the same beam spot size (1 cm), impact point and polar angle.

3 Results

3.1 Light yield

In the last three years an extensive R&D program was carried out to optimize the light yield of the Tile calorimeter. In particular, the transmission and light yield of the tiles, the numerical aperture of the fibres, and the geometry of the tile/fibre coupling have been optimized [3].

The number of photoelectrons for the prototypes constructed in the years 1993 to 1995 was determined using three different methods: neutral filters [2], muon data and laser information. In this section we report on a study done with 150 GeV muons impinging on the Tile calorimeter at a polar angle $\theta = 90^o$, where the muons are incident perpendicular to the scintillator surfaces.

The photoelectron yield normalized to a deposited energy, N_{pe} per GeV per cell, can be determined as [4]:

$$N_{pe} = C \left(\frac{Q_c}{\sigma_c}\right)^2 \frac{1}{Q_c} \alpha_e \qquad (1)$$

where Q_c is the two-PMT charge per cell (in pC), and σ_c is the *rms* value of the difference of the signals of the two PMTs which arises from photostatistics. The parameter C is a factor to correct for statistical fluctuations in the first few dynodes of the PMT. Here C was taken to be 1, whereas Ref. [4] uses C = 1.11. In Ref. [5] a slightly different formula than Eq. (1) was applied to the same data, with comparable results. In the above the conversion of muon response (in pC) to energy (in GeV) was made on the basis of the calibration constant found with electrons, α_e. This conversion factor, α_e, is energy independent since it is determined using electrons, dividing the digitized calorimeter signal by the energy of the incident electron beam. $\alpha_e = 5.59$ pC/GeV at 10^o incidence [6].

The photoelectron yield obtained for the different size tiles from different depths is shown in Fig. 3. Each data point corresponds to the average summed response from 11 or 12 tiles in a cell. Since small tiles are coupled to long fibers,

and large tiles are coupled to short fibers, the product of attenuations results in a rather uniform light yield in depth. Also shown in the figure are the light yields for earlier 1993 and 1994 prototypes, and the progressive improvements made. The combined effect of the tiles' quality, the use of double clad fibres and better geometry on the tile/fibre coupling has increased the photoelectron yield by an overall factor of about 2.5, from 24 pe/GeV to 64 pe/GeV [3].

A comparison of these results with an earlier technique using electrons at $\theta = 90^o$, measuring the change in resolution when the light on the PMT is reduced by means of neutral density filters, yields consistent values. For the 1993 module prototypes, this method results in $N_{pe} = 20$ and 25 pe/GeV for tiles #10 and tile #6 respectively, in good agreement with values obtained using Eq. (1).

3.2 Muon signal

The energy lost in the Tile calorimeter by 150 GeV muons at a polar angle of $\theta = 10^o$ is shown in Fig. 4a for the full calorimeter depth (8.9 λ) and in Fig. 4b for the first longitudinal sampling (1.5 λ) only. The energy loss spectrum approximately follows a Landau distribution, but with large tails at high energies caused by radiative processes (Bremsstrahlung, electron-positron pair production) as well as energetic δ-rays.

The simulated energy losses in the Tile calorimeter are also shown in Fig. 4 with and without instrumental effects. The spectra normalization to the data is made to obtain the same most probable value (MOP) of energy loss at 50 GeV. The simulations incorporating the instrumental effects agree well with the experimental data. The broadening of the distribution due to fluctuations in instrumental effects (mostly photoelectron statistics) is most evident in the first sampling, which is the thinnest longitudinal compartment (30 cm or 1.5 λ).

The pedestal distribution after subtraction of its average value is also shown in Fig. 4. The width of this distribution corresponds to a noise of about 40 MeV/cell. This value contains a surprisingly high amount of correlated noise contribution, unlike data taken on a previous beamline and with different readout electronics wherein the noise per cell was much lower (about 20 MeV/cell) [7]. Even in these less-than-optimal conditions the pedestal is well separated from the muon signal.

In Fig. 5 experimental data on the muon lineshape from the three generations of Tile calorimeters yielding 24 pe/GeV, 48pe/GeV and 64 pe/GeV are shown. The signals in the entire calorimeter and in the first sampling are shown. A broadening of the spectrum is clearly visible in the first sampling but not in the full calorimeter; only a small broadening of the muon line shape is observed in the full module with 24 pe/GeV.

These results indicate that a light yield as low as 48 pe/GeV will not significantly deteriorate the quality of the muon measurements. Nevertheless, ageing effects and radiation damage will reduce the light yield and in the long term the calorimeter performance will be more robust with the highest light output.

3.3 Response uniformity

The uniformity of the response to muons using test beam data has been studied as a function of displacements of the point of incidence of the beam described by the coordinates (θ, ϕ, z). A span of 60 cm in z on the calorimeter face was scanned with 180 GeV muons at a polar angle of $\theta = 10^o$. The results of the scan are shown in Fig. 6a and 6b. The signal response is quite uniform with an RMS spread of 1.8%.

The uniformity in the vertical (y) direction (ϕ scan) has been studied using 150 GeV muons at $\theta = 10^o$. Fig. 7a shows the signals in the two center modules below and above the interface between them (the "crack") as a function of the vertical displacement y ($\Delta\phi = 0.56^o$ corresponds to a vertical displacement of 1 cm in y). The y coordinate is measured from the crack, in a plane perpendicular to the crack plane. The sum of the signal of the two modules is also shown. Signals have been normalized to the signal at the centre of module three.

There is a drop in the signal of about 60% at y = 0 cm, where there is a small gap between scintillators to allow fibre insertion. In Fig. 7b the distribution of the normalized signals is shown together with a Gaussian fit (excluding the points in the crack) with a $\sigma = 2.5\%$. Outside the crack region a rather uniform response over the full module surface is observed. A non-uniform response observed in the past has been eliminated in the present prototypes by means of a better tile masking and tile/fibre coupling geometry.

The polar angular dependence of the muon signals has also been studied using 200 GeV muons. The signal, normalized for the same path length, is shown in Fig. 8 as a function of the incident polar angle θ for data and MC simulations. A dependence of the response on the polar angle within 5 % is observed. This effect is also well reproduced by the MC. A similar behaviour is observed with pions [3]. This can be understood by alignment effects in the staggered tile/iron geometry, because the sampling fraction can change rapidly at small polar angles as will be discussed in Section 4.2.

3.4 Energy dependence of the muon response

The energy loss in the calorimeter as a function of incident energy was studied with muons traversing the Tile calorimeter prototypes at a polar angle of $\theta = 10^o$ using both experimental data and MC simulations with all instrumental effects properly included.

The energy loss measured in the Tile calorimeter is shown in Fig. 9 for both data and simulation, for muon energies of 20, 100 and 200 GeV and for simulation only at 5 GeV. As expected, the most probable energy loss grows slowly with incident energy as well as an enhancement in the tail of the distribution. Both effects are well reproduced by the simulation. The most probable values were obtained from a fit of the energy loss distributions to a Moyal function [8]. This asymmetric distribution is characterized by a width parameter σ_M which is the rms deviation of the function from its peak value. A truncated mean value of energy loss is found by calculating the mean of these distributions at values less than 5 σ_M.

The mean and the most probable values of the energy losses measured at $\theta = 10^o$ at several beam energies are shown in Fig. 10 and in Table 1. The most probable values vary from 2.26 to 2.85 GeV for incident energies between 10 and 300 GeV, or equivalently by approximately 7% per 100 GeV/c increase in muon momentum over the range of 50 to 300 GeV/c. The truncated mean increases more steeply, at approximately 10% per 100 GeV/c increase in muon momentum.

The peak muon energy deposition in the calorimeter of about 2.5 GeV can be compared to the expected energy deposition of minimum bias events per bunch-crossing for nominal luminosities ($10^{34} cm^{-2} sec^{-1}$) at the LHC, which amounts to ~ 0.2 GeV into a $\Delta\eta \times \Delta\phi = 0.1 \times 0.1$ calorimeter cell. This gives a comfortable margin for detecting isolated muons even at the highest luminosity (S/B ~ 10).

3.5 The e/μ and e/mip ratios; muon and electron sampling fractions

The e/μ ratio is defined, following ref. [9], as the ratio of the electron and muon energy to charge conversion factors (α_e/α_μ) in the Tile calorimeter. Using e/μ the energy lost by muons in the calorimeter can be obtained as

$$E_\mu = \frac{e}{\mu} E_{exp} = \frac{e}{\mu} \frac{Q_\mu}{\alpha_e} \tag{2}$$

where $E_{exp} = Q_\mu/\alpha_e$ are the experimentally determined muon energy losses as given in Table 1. Q_μ is the muon charge.

The energy lost in the calorimeter is calculated using the energy-independent electron scale factor α_e. However, the exact energy deposited by muons will be overestimated by about 10% since muons and electrons do not have the same sampling fraction.

The e/μ ratio differs from 1 because in a sampling calorimeter the electron and muon sampling fractions S_e and S_μ differ from that of a minimum ionizing particle (mip) for the following reasons:

- for electrons, the low-energy photon component of the shower is very inefficiently sampled [10]. Therefore, in general $S_e < S_{mip}$.

- for muons, S_μ is energy dependent because of the energy-dependent difference of dE/dx between scintillator and absorber, and because of the increasing importance with energy of the radiative energy loss processes which are sampled essentially as S_e.

These effects are very sensitive to the atomic number Z of the absorber and scintillator components and to their respective thicknesses, particularly for high-Z absorbers such as Pb or U.

To calculate e/μ for the Tile calorimeter the same simulation code mentioned above has been used, assuming that the code accurately reproduces the details of the ionization and radiation processes. The assumption is justified by the close agreement obtained between data and simulation in both the deposited energy spectra (Fig. 9) and in the dependence on energy of most probable and mean energy losses (Fig. 10 and Table 1). This allows us to replace E_μ with E^{tot}_{MC}, the simulated energy loss in the whole calorimeter, in Eq. (2) to obtain e/μ for each muon energy:

$$e/\mu = \frac{E^{tot}_{MC}}{E_{exp}} \tag{3}$$

The most probable values obtained from Moyal fits to the distributions of E^{tot}_{MC} and E_{exp} have been used to calculate e/μ; the results are given in Fig. 11 and Table 3.

The ratio e/μ is 0.91 ± 0.01 and independent of energy (within errors) up to about 150 GeV. At higher energies e/μ approaches 1 as expected as the relative weight of radiative processes increases at higher energy.

The e/mip parameter, the ratio of the response of a calorimeter to electromagnetic showers to that of minimum ionizing particles depositing the same energy, was also determined. This parameter is important to understand the response of a calorimeter to hadrons [10] as well. e/mip can be written as a first approximation as

$$e/mip = \frac{\alpha_e}{Q_\mu/E_{mip}} = \frac{E_{mip}}{E_{exp}} \tag{4}$$

where E_{exp}, the most probable value of the muon energy loss at $\theta = 10^o$, is taken from Table 1 and the most probable energy E_{mip} lost in the calorimeter by a mip at this angle of incidence is calculated from early Particle Data Group (PDG) data [11] and our calorimeter geometry; it is 1.545 GeV.

However for a highly relativistic particle (for example at 10 GeV, $\beta\gamma$=95, whereas for a mip $\beta\gamma$=3.5) one needs to correct E_{exp} for the relativistic rise in dE/dx. This can be done by normalizing Eq. (4) by the ratio of the energy deposited in the scintillator by a high energy muon to that of a mip. The energy deposited by a mip in the scintillator, E^{scint}_{mip}, is obtained from the PDG data,

while the energy deposited by a high energy muon, E_{MC}^{scint}, is derived from our simulation. Thus we can write as a better approximation

$$e/mip = \frac{E_{mip}}{E_{exp}} \frac{E_{MC}^{scint}}{E_{mip}^{scint}} = \frac{1}{S_{mip}} \frac{E_{MC}^{scint}}{E_{exp}} \tag{5}$$

The calculation was performed for both the most probable and the mean values of the energy losses. Using the earlier PDG values for most probable mip energy losses, and recent PDG data [12] for mean energy losses in the scintillator and in the entire calorimeter, the values shown in Fig. 11 and in Table 3 were obtained.

The e/mip ratio is seen to be roughly independent of energy within errors, as it should be. The values of e/mip averaged over the observed energies are 0.85 and 0.78 when most probable and mean values of the energy losses are used respectively. These two values differ almost entirely due to the result of the calculations of sampling fraction, S_{mip}, using most probable and mean energy loss, which yield 0.0337 and 0.0362 respectively.

Using the average of the above values and their difference as an estimate of the systematic uncertainty on e/mip, a value of

$$e/mip = 0.81 \pm 0.03 \tag{6}$$

is obtained. The most probable and mean values of E_{exp}, E_{MC}^{tot} and E_{MC}^{scint} used in calculating e/μ and e/mip are given in Table 2.

In view of the systematic uncertainties on the e/mip value, and of the agreement of the simulations with the experimental results, it appears useful to quote effective values of the muon and electron sampling fractions obtained from the Monte Carlo simulation. The muon sampling fraction was calculated as the mean of the event-by-event ratio of the energies deposited in the scintillator and in the entire calorimeter. This ratio, unlike its components, has a nearly Gaussian distribution. The sampling fraction *vs.* muon energy is also given in Table 3. It is seen to decrease smoothly from 3.2% at 10 GeV to 3.0% at 300 GeV. The low-energy ($\beta\gamma_{min}$) and high-energy limits of the muon sampling fraction are S_{mip} and S_e respectively. The electron sampling fraction S_e can be obtained from the muon sampling fraction by multiplying it by the e/μ ratio. For the Tile calorimeter $S_e = 2.9\% \pm 0.1\%$.

4 Monte Carlo study of the muon energy losses

As mentioned in the Introduction, fluctuations in muon energy losses can be an important source of error in measuring the muon momentum, and in fact dominate the ATLAS muon momentum resolution below 30 GeV/c. The larger fluctuations, which are due to hard radiative processes and energetic δ–rays, are characterized by secondaries which are rather effectively sampled in the Tile calorimeter because they typically traverse several iron-scintillator interfaces. This leads to a high degree of correlation between the energy deposited in the iron (about 97% of the total, as discussed in the previous section) and the signal in the scintillators. Using our simulation to calculate the energy loss in both the iron absorber and the scintillator, we show in Fig. 12 this correlation for several incident muon energies. The correlation is already evident in the high-energy end of the signal produced by 10 GeV muons, while for lower incident energies softer ionization secondaries dominate and no correlation exists. Consequently for $E_\mu > 10$ GeV the muon energy loss in the calorimeter can be estimated, event by event, from the energy loss in the scintillator.

A detailed study of the correlation, using the prototype's simulation and applying it to the ATLAS configuration when appropriate, is described in this section. The possible improvement in measuring momenta of isolated muons is discussed.

4.1 Correlations between energy losses in the iron and in the scintillator in the Tile calorimeter prototype

To study the correlation between the energies lost in the absorber and active material, the energies lost event by event in iron and scintillator were calculated and divided each by the corresponding sampling fractions, 1-S_μ and S_μ. The simulated values of S_μ in Table 3 were used. The distributions of the differences of the scintillator and iron values are shown in Fig. 13, together with Gaussian fits within $\pm 2\sigma$. The mean values of the differences are very close to zero as expected. The spread of the distribution of the differences, measured by σ, is a good representation of the error in reconstructing the energy loss in the calorimeter using the scintillator signal. Plots of σ *vs.* muon energy are given in Fig. 14 (black dots) and contrasted with the widths σ_M obtained from a Moyal fit to the total energy losses in the calorimeter (stars). The values from the fits are given in Table 4a.

For muon momenta above 100 GeV the energy loss fluctuations can be reconstructed rather precisely using the scintillator signals. The σ of the difference distribution is about 400-500 MeV (0.2-0.3%) whereas, in contrast, σ_M of the energy loss distribution is larger and is about 500-1300 MeV.

At muon energies $\lesssim 20$ GeV the σ of the difference distribution rapidly increases from 1.6% (318 MeV) at 20 GeV/c to 5.9% (295 MeV) at 5 GeV/c. We

can see from Table 4 that at $\lesssim$ 20 GeV the average energy loss has better resolution than does the difference distribution, and thus is a better approximation to the true energy loss than an event-by-event estimate based on the scintillator information. In this energy range the fluctuations of the energy loss in the calorimeter are the dominant factor in the ATLAS muon momentum resolution (Fig. 1).

Above 100 GeV the momentum resolution of the ATLAS muon spectrometer is increasingly dominated by tracking and alignment errors [1] (see again Fig. 1); therefore precise reconstruction of the muon energy loss in the calorimeter is only useful for events with large or even "catastrophic" energy losses. The limit on correlating such losses with the scintillator signals can be estimated from Fig. 13, where tails due to very large energy losses in the absorber are seen to develop at the higher incident momenta. The fraction of events 3σ or more above the peak is 1% at 10 GeV and 5 to 6% above 150 GeV (see Table 4a).

It is worth to repeat that if the absorber consisted of a higher Z material like lead, the average energy losses in the calorimeter (and their fluctuations) would be much larger than in an iron/scintillator calorimeter with the same thickness in interaction lengths and sampling fraction [9]. In addition, the correlation of the energy losses in the absorber and the sampling material would be weaker.

4.2 Extension to the ATLAS configuration

In the ATLAS configuration, the total amount of material in front of the muon spectrometer will be 107 X_0 (10.6 λ) at $\eta = 0$. Of the materials in ATLAS, the active parts of Lead-LAr electromagnetic calorimeter and the Tile calorimeter represent 25 X_0 and 68.7 X_0 respectively. Thus if both the LAr and Tile calorimeters can be used to identify muons, 88% of the total 107 X_0's is sampled while if only the Tile calorimeter is used, then only 64% of the volume is sampled.

The effect of sampling the muon energy loss over only part of the volume has been studied using the MC simulation of the Tile calorimeter prototype. Using only the information from the first three depth samplings only 67% of the total energy loss is sampled (see section 2), a situation which is not too far from that of ATLAS at $\eta = 0$. The results of the simulation are shown (open circles) in Figs. 14a, 14b and Table 4b. The precision in the correlation degrades by about 30% at all muon momenta. By simply enabling two or more contiguous depth sample readouts in the prototype simulation we can estimate the degradation of the correlation as a function of the fraction of material sampled. Results for the prototype are shown in Fig. 15 for muon momenta of 10 GeV/c and 300 GeV/c. If no information is available from the LAr calorimeter, we estimate the degradation at about 30-35%. But if isolated muons are detected in both the LAr and Tile calorimeters, the resulting degradation becomes only about 3%.

A peculiar effect due to the Tile calorimeter construction needs consideration in ATLAS. For muon trajectories close to $\eta = 0$ one expects a modulation

along the z direction of the amount of iron traversed by a muon. This is due to the alternating layers of iron absorber plates and iron absorber interspersed with scintillator tiles. The impact points with the maximum signal in the scintillator correspond to the smallest energy deposition in iron. In the prototype calorimeter this effect disappears for angles of more than 7^o to the $\eta = 0$ plane. The modulation is seen in the MC as illustrated in Fig. 16 for 180 GeV muons entering the Tile calorimeter at $\theta = 0^o$, the worse case. The period of the oscillation is 9 mm, which corresponds to the staggered tile/iron geometry structure. As expected the modulation is no longer observable at $\theta = 10^o$ (see Fig. 16). This effect is maximal in the prototype, where tiles all have the same depth along the muon trajectory but will be smaller in the ATLAS calorimeter since tile sizes have been chosen to minimize this effect.

4.3 The muon momentum resolution after event-by-event reconstruction of the energy losses

Several algorithms to calculate the muon energy loss on an event-by-event basis have been considered. Fig. 17 shows energy losses in the iron versus losses in the scintillator for several incident muon energies. The correlation can be parameterized in the form:

$$E_{Fe} \;=\; a_1 \times E_{scint}^{-a_2} + p_1 \times E_{scint}^{p_2}, \tag{7}$$

where p_1 and p_2 are polynomials with $p_1 = a_3 + a_4 \times E_\mu$ and $p_2 = a_5 + a_6 \times E_\mu + a_7 \times E_\mu^2$. E_μ is the incident muon energy in GeV and a_n $(n = 1 \ldots 7)$ are constants. The function is drawn in the figure for $E_\mu = 300$ GeV. This form adequately describes the correlation for muons between 10 and 300 GeV. For relatively large scintillator signals ($E_{scint} \gtrsim 100$ MeV) the slope of the correlation E_{Fe} versus E_{scint} is independent of the incident muon energy and is approximately equal to the sampling fraction of electrons. On the other hand, at smaller scintillator signals ($E_{scint} \lesssim 100$ MeV) the correlation is somewhat dependent on incident muon energy. This parameterization is used to correct the muon momenta for the energy losses in the calorimeter on an event-by-event basis. The result is compared to the distribution obtained by correcting simply for the most probable value of the total energy loss of muons in the calorimeter.

The case of 50 GeV/c muons will be illustrated in some detail. The effect of the simpler approach is shown in Fig. 18a. The momentum peaks at the correct energy value but has a large low-energy tail. In ATLAS, the multiple scattering and the measurement/alignment error in the muon chambers give additional contributions to the momentum resolution.

The distribution in Fig. 18a has been smeared by an energy-dependent function to include the latter contributions. The result is shown in Fig. 18b. A gaus-

sian fit between $\pm 2\sigma$ is also shown in the figure. It gives σ=782 MeV (σ/p=1.6%), with 4.7% of the events in the low-energy tail which is defined as 3σ or more below the peak.

The muon momenta reconstructed with the parameterization described above are shown in Fig. 18c. After smearing (see Fig. 18d), the Gaussian fit gives a slightly lower σ than that obtained with the first method (723 MeV or 1.4% instead of 782 MeV). The percentage of events in the low-energy tail is substantially reduced to 1.7% .

A third method, based on a combination of the first two, has been considered: events which deposit little energy in the scintillator($E_{scint} \leq 80$ MeV, see Fig. 17) are corrected with the most probable energy loss (first method), while the events with $E_{scint} > 80$ MeV are corrected by the energy loss estimated event by event (second method). The results are shown in Fig. 18e before smearing. An improvement is seen in the value of σ while after smearing (Fig. 18f), the result is similar to that obtained with method 2.

The same study was carried out with 20 and 300 GeV muons; the results are given in Table 5. At 300 GeV, the contribution from the errors in the muon spectrometer dominates the muon momentum resolution and does not allow to profit from the precise reconstruction of the muon energy loss obtained using the scintillator information. The advantage of the method is limited to a significant reduction of the low-energy tail.

At 20 GeV the correlation between the energy loss in the iron and in the scintillator is not good enough to reduce the width of the error distribution; however a reduction in the low-energy tails is still seen.

These results were obtained by sampling the entire thickness of the calorimeter. Reducing the sampled fraction to 67% does not affect the width of the reconstructed momentum distributions but increases the fraction of events in the low-energy tails (from 1.4% to 4.1% at 20 GeV using method 3).

In conclusion, using the calorimeter information to reconstruct the ATLAS muon momenta will reduce tails in the momentum error distribution at all muon energies. A small improvement of the width of the error distribution can only be obtained at intermediate muon momenta (around 50 GeV). At lower momenta the information from the scintillator is typically not useful, while at high momentum the measurement/alignment error in the muon chambers, together with the multiple scattering, dominates the resolution.

5 Summary and Conclusions

In closing, it may be worth to briefly restate the main results of this study:

- With the last generation of calorimeter prototypes a light yield of about 64 photoelectrons per GeV deposited in the calorimeter has been obtained. This yield (or even a slightly lower one) is sufficient to observe isolated muons traversing the thinnest calorimeter segment with no degradation of the spectrum of the signal.

- The most probable muon signal in the whole calorimeter is about a factor of 10 higher than the expected noise from minimum-bias events at the nominal luminosity of the LHC. Therefore isolated muons down to approximately 2 GeV should be visible in ATLAS using just calorimeter information.

- The observed energy loss spectra of muons from 10 GeV/c to 300 GeV/c are seen to be in excellent quantitative agreement with Monte Carlo simulations which account in detail for all muon energy loss processes and for instrumental effects. The observed agreement is useful to precisely calculate the muon energy losses at each muon energy, both on the average and on an event-by-event basis.

- The (most probable and average) ratio of electron and muon response of the calorimeter for equal deposited energies (the e/μ ratio) is estimated as a function of energy. This ratio allows to precisely obtain the average or most probable energy losses of muons. As expected this ratio approaches 1 as the muon energy increases.

- The fluctuations of the energy losses suffered by muons in the calorimeter can be rather precisely recovered using the scintillator signals. After accounting for all measurement errors, the resolution on the muon momentum obtained by an event by event correction algorithm is not appreciably better than can be obtained just by correcting for the most probable energy loss; however the event by event correction recovers most of the "catastrophic" energy losses and thereby significantly improves the losses and biases due to "low-energy tails".

In summary, it is shown in this paper that the Tile calorimeter is capable of providing useful information on muon identification, which constitutes one of the crucial signatures for many physics channels at the LHC.

Acknowledgements

The construction of three generations of calorimeter prototype modules within a very short time was only possible with substantial contributions by the technical staff of the collaborating institutions. We deeply thank them for their support.

Financial support is acknowledged from the funding agencies of the collaborating Institutes.

Finally, we are grateful to the staff of the SPS, and in particular to K. Elsener, for the excellent beam conditions and assistance provided during our tests.

References

[1] ATLAS Technical Proposal, CERN/LHCC/94-43 LHCC/P2.

[2] F. Ariztizabal *et al.*, Nucl. Instr. and Meth. **A349** (1994) 384.

[3] E. Berger *et al.*, CERN/LHCC 95-44, LRDB status report/RD34, 1995.

[4] A. Bernstein *et al.*, Nucl. Instr. and Meth. **A336** (1993) 23 and **A262** (1987) 229.

[5] J. Proudfoot and R. Stanek, ATLAS Internal Note, TILECAL-NO-66[1] following the formalism found in K. Yasuoka *et al.*, Nucl. Instr. and Meth. **A267** (1988) 330.

[6] J. A. Budagov *et al.*, ATLAS Internal Note, TILECAL-NO-72.

[7] M. Cobal *et al.*, ATLAS Internal Note, TILECAL-NO-67.

[8] E. Moyal, Phil. Mag. **46** (1955) 263.

[9] A. Acosta *et al.*, Nucl. Instr. and Meth. **A320** (1992) 128.

[10] R. Wigmans, Nucl. Instr. and Meth. **A259** (1987) 389.

[11] Particle Data Group, Phys. Lett. **B170** (1986) 38.

[12] Particle Data Group, Phys. Rev. **D50** (1994) 1173.

[1] The TILECAL notes can be found on WWW at
http://atlasinfo.cern.ch/Atlas/SUB_DETECTORS/TILE/tileref/tinotes.html
in postscript format.

Muon line shape characteristics				
	Exp		MC	
E_{beam} (GeV)	MOP (GeV)	$width$ (GeV)	MOP (GeV)	$width$ (GeV)
10	2.26	0.51	2.29	0.49
20	2.28	0.55	2.32	0.53
50	2.40	0.59	2.40	0.62
100	2.51	0.75	2.50	0.74
150	2.61	0.85	2.59	0.85
200	2.65	0.94	2.69	0.97
300	2.85	1.28	2.87	1.17

Table 1: Line shape parameters of the energy loss spectra of muons at $\theta = 10^o$. The most probable (MOP) value and width (σ_M) were obtained from a Moyal fit to the signal distributions truncated at $+5\ \sigma_M$. The MC results normalized to the experimental data at 50 GeV are also shown.

Most probable energy losses in the Tile calorimeter			
E_{beam} (GeV)	E_{exp} (GeV)	E_{MC}^{sc} (MeV)	E_{MC}^{tot} (GeV)
10	2.256 ± 0.012	65.05 ± 0.11	2.051 ± 0.001
20	2.277 ± 0.008	65.97 ± 0.11	2.094 ± 0.002
50	2.401 ± 0.013	68.12 ± 0.13	2.174 ± 0.003
100	2.510 ± 0.011	70.93 ± 0.15	2.291 ± 0.003
150	2.612 ± 0.007	73.49 ± 0.18	2.399 ± 0.006
200	2.646 ± 0.027	76.42 ± 0.14	2.521 ± 0.008
300	2.850 ± 0.024	81.33 ± 0.23	2.765 ± 0.012
Mean energy losses in the Tile calorimeter			
E_{beam} (GeV)	E_{exp} (GeV)	E_{MC}^{sc} (MeV)	E_{MC}^{tot} (GeV)
10	2.530 ± 0.012	72.23 ± 0.13	2.197 ± 0.003
20	2.599 ± 0.008	74.06 ± 0.15	2.270 ± 0.003
50	2.784 ± 0.013	77.68 ± 0.17	2.410 ± 0.004
100	2.980 ± 0.011	83.25 ± 0.22	2.622 ± 0.006
150	3.168 ± 0.007	88.19 ± 0.26	2.820 ± 0.008
200	3.283 ± 0.027	93.92 ± 0.31	3.039 ± 0.010
300	3.610 ± 0.024	102.96 ± 0.38	3.452 ± 0.013

Table 2: The most probable and mean energy losses in the Tile calorimeter. Experimental and Montecarlo data are presented. For Montecarlo two values are shown: energy deposited in scintillator and energy deposited in the whole calorimeter. The most probable loss was obtained from a Moyal fit to the signal distributions truncated at $+5\ \sigma_M$. Mean energy loss was obtained from the same distributions truncated at $+5\ \sigma_M$.

The e/μ and e/mip ratios and the muon sampling fraction				
E_{beam} (GeV)	e/μ MOP	e/mip MOP	e/mip mean	S_μ (%)
10	0.909 ± 0.005	0.856 ± 0.005	0.789 ± 0.004	3.238 ± 0.004
20	0.920 ± 0.003	0.860 ± 0.003	0.787 ± 0.003	3.184 ± 0.004
50	0.906 ± 0.005	0.842 ± 0.005	0.771 ± 0.004	3.148 ± 0.004
100	0.913 ± 0.004	0.839 ± 0.004	0.772 ± 0.003	3.101 ± 0.005
150	0.918 ± 0.003	0.835 ± 0.003	0.769 ± 0.003	3.067 ± 0.005
200	$0.953 \pm .010$	0.857 ± 0.009	0.790 ± 0.007	3.041 ± 0.005
300	0.970 ± 0.009	0.847 ± 0.008	0.788 ± 0.006	2.984 ± 0.005

Table 3: The e/μ and e/mip ratios and muon sampling fraction as a function of the incident muon energy calculated for an angle of incidence $\theta = 10^o$. The most probable (MOP) and mean values used for energy loss in the e/mip calculation are given.

Fluctuations of the muon energy loss in the Tile calorimeter				
a) Full calorimeter (=80.5X_0) sampled				
E_{beam} (GeV)	σ (MeV)	σ/E_{beam} (%)	Number of events $\geq 3\sigma$ (%)	σ_M of E_{loss} (MeV)
5	295	5.90	0.4	196
10	310	3.10	0.9	236
20	318	1.59	1.6	274
50	342	0.68	2.6	357
100	377	0.38	4.3	505
150	420	0.28	4.7	641
200	432	0.22	5.5	784
300	525	0.17	5.8	1082
b) 67% of full calorimeter(=54 X_0) sampled				
E_{beam} (GeV)	σ (MeV)	σ/E_{beam} (%)	Number of events $\geq 3\sigma$ (%)	σ_M of E_{loss} (MeV)
5	391	7.82	0.1	196
10	387	3.87	1.4	236
20	394	1.97	3.6	274
50	409	0.82	3.6	357
100	492	0.49	5.0	505
150	511	0.34	6.3	641
200	603	0.30	6.5	784
300	676	0.23	9.4	1082

Table 4: The precision (σ in MeV and in percent of the incident muon energy) of the difference of the energy loss in iron and in scintillator corrected for their respective sampling fractions. Column 5 shows the σ_M of Moyal fit of the true total energy loss in the calorimeter. Results in part (a) are obtained when the full calorimeter length is sampled by the scintillator (80.5 X_0), in part (b) when only 67% of the calorimeter is sampled by the scintillator (the scintillator signal from sampling 4 was not considered) but the muon still travels the full calorimeter length.

Muon momentum resolution with all effects included									
	20 GeV			50 GeV			300 GeV		
Correction Method	σ_p MeV	σ_p/p (%)	tail$\leq 3\sigma$ (%)	σ_p MeV	σ_p/p (%)	tail$\leq 3\sigma$ (%)	σ_p MeV	σ_p/p (%)	tail$\leq 3\sigma$ (%)
1) Mean E_{loss}	349	1.8	7.0	782	1.6	4.7	8470	2.8	1.53
2) $E_{loss\ evt-evt}$	356	1.8	1.7	723	1.4	1.7	8450	2.8	0.3
1) for $E_{Sc}\leq 80$ MeV 2) for $E_{Sc}\geq 80$ MeV	356	1.8	1.4	727	1.5	0.9	8450	2.8	0.3

Table 5: The expected muon momentum resolution and fraction of events in tails below 3 σ for 20, 50 and 300 GeV muons after traversing the Tile calorimeter prototype. The results take into account the contribution of the multiple scattering and the measurement/alignment error in the muon chambers. Three different methods were used to correct for the energy losses in the calorimeter. Method 1 adds to each event the most probable value of the energy lost in the calorimeter (2.32, 2.40 and 2.8 GeV for 20, 50 and 300 GeV muon respectively). Method 2 corrects on an event by event basis for the energy loss in the calorimeter. Method 3 is a mixture of the 2 first methods, e.g. method 1 for events with $E_{scintillator} \leq 80$ MeV and method 2 for events with $E_{scintillator}$ above 80 MeV.

Figure 1: Momentum resolution at zero rapidity, as a function of the muon momentum. The figure shows the contribution from energy loss fluctuations in the calorimeter, multiple scattering in the precision and trigger chambers, and the measurement error including alignment contribution (Figure taken from Ref. 1).

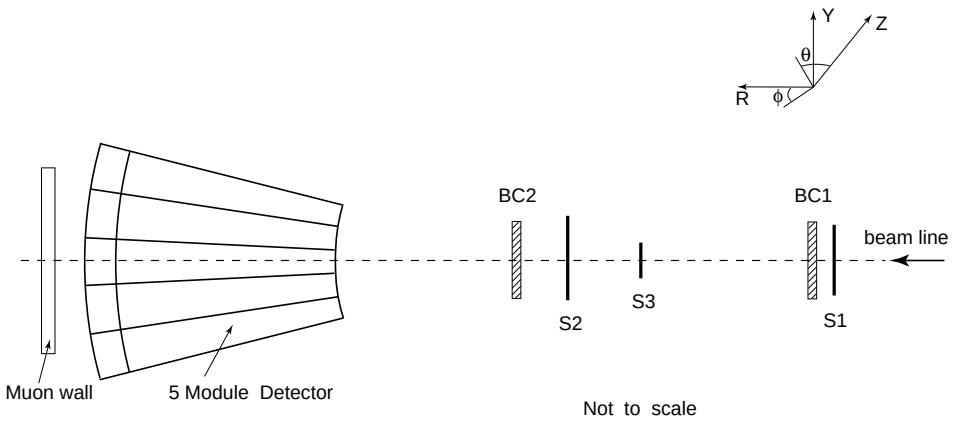

Figure 2: A sketch of the layout of the prototype Tile calorimeter modules in the CERN H8 beamline. S1,S2 and S3 are beam defining scintillators and BC1 and BC2 are wire chambers to determine the incident angle.

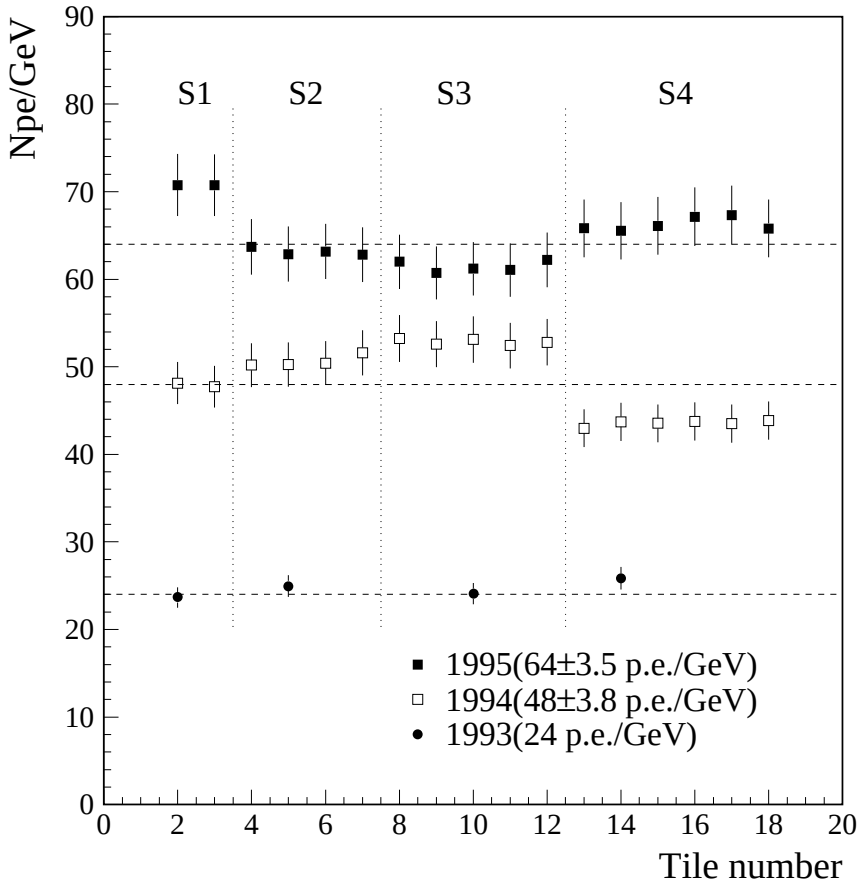

Figure 3: Number of photoelectrons per GeV per cell (2 PMTs) as a function of the tile number, or tile position in depth. Experimental values are given for Tile calorimeter prototypes built in the years 1993, 1994 and 1995. Tile size increases from tile number 1 to 18.

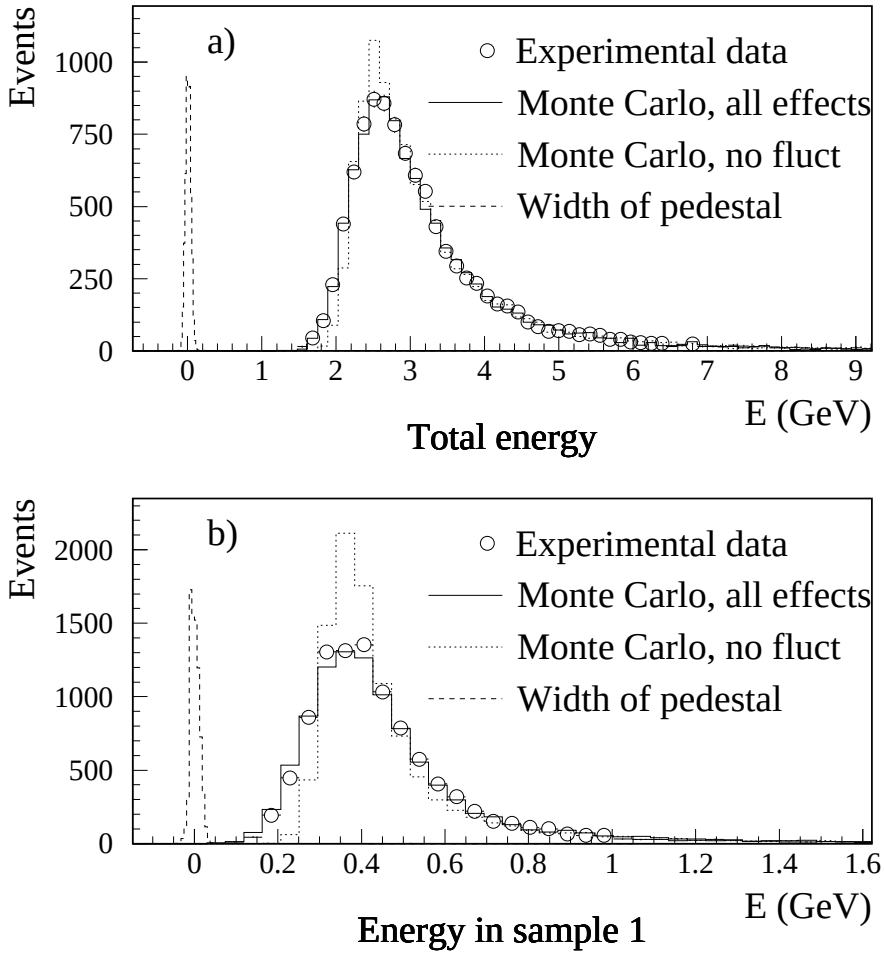

Figure 4: Energy loss of 150 GeV muons traversing (a) the full Tile calorimeter depth (9 λ), (b) the first sampling (1.5 λ). The open circles are experimental data while the dashed and full lines are simulation results with and without instrumental fluctuations (PMT noise and photoelectron statistics), respectively. The pedestal width is also shown.

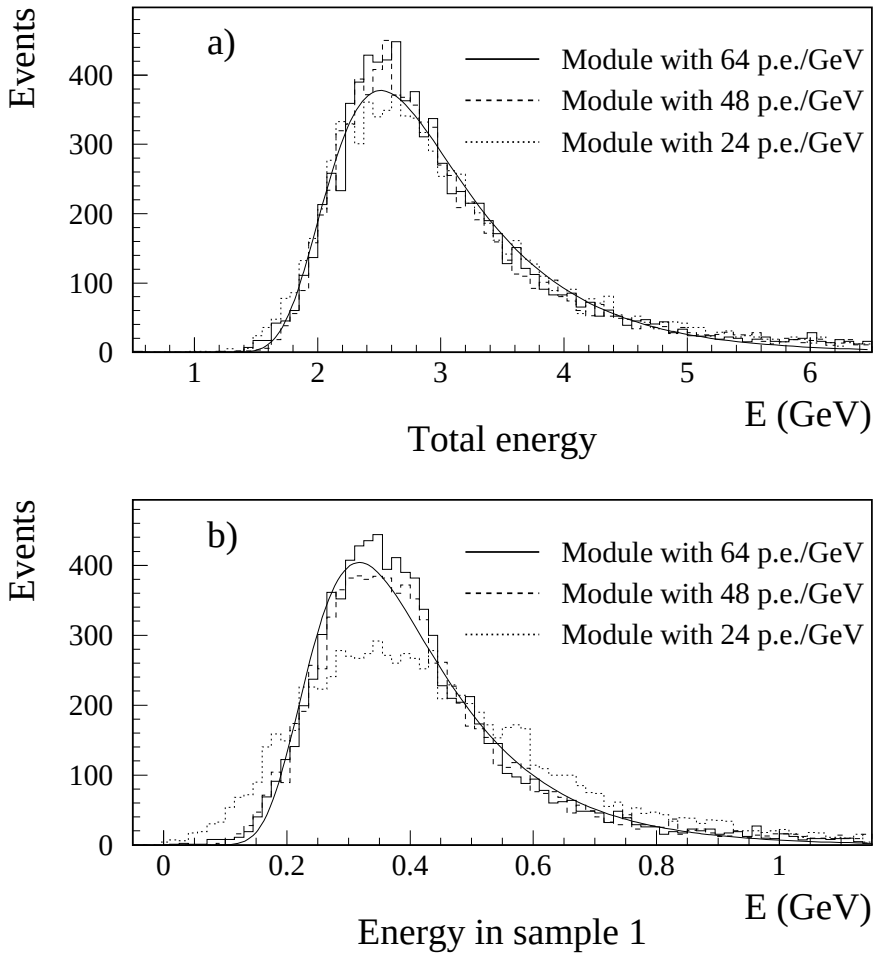

Figure 5: Experimental data on the energy loss of 150 GeV muons at $\theta = 10^o$ traversing (a) the full calorimeter length (9 λ), (b) the first sampling (1.5 λ). Data from three prototypes with different light yields (24, 48 and 64 pe/GeV per cell) are shown. A Moyal fit applied on the module with the highest light yield is shown as the full curve.

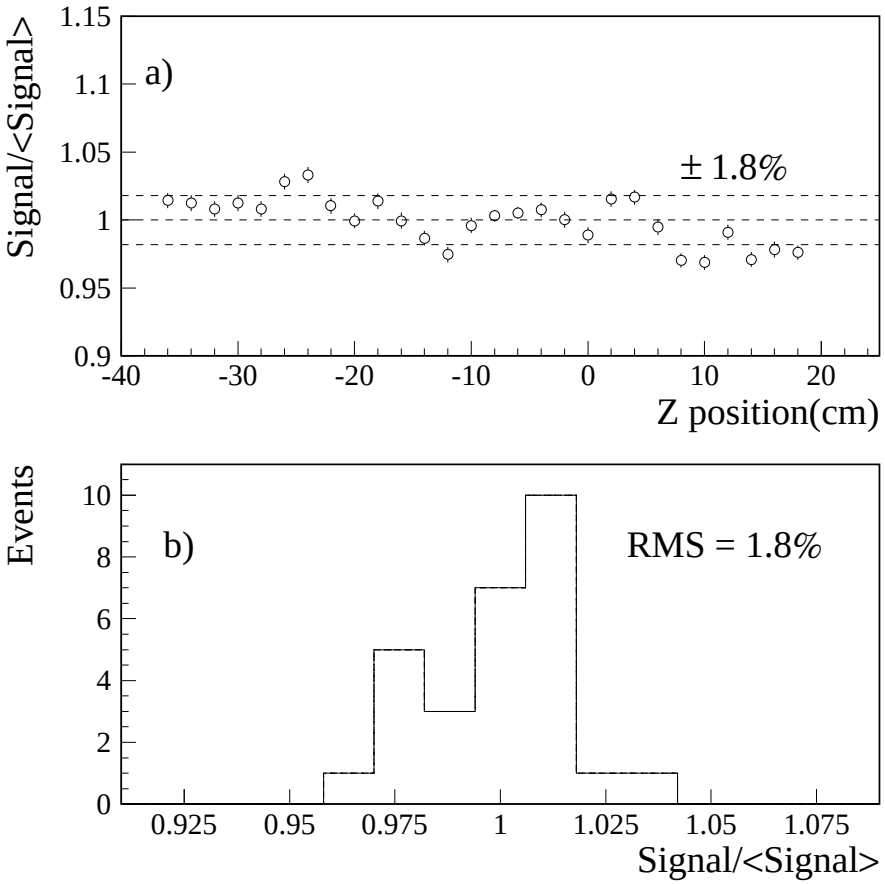

Figure 6: (a) Uniformity scan along the z direction using 180 GeV muons impinging on the Tile calorimeter at $\theta = 10^o$. (b) The resultant distribution of the mean of the muon signal relative to the average. Experimental data is shown.

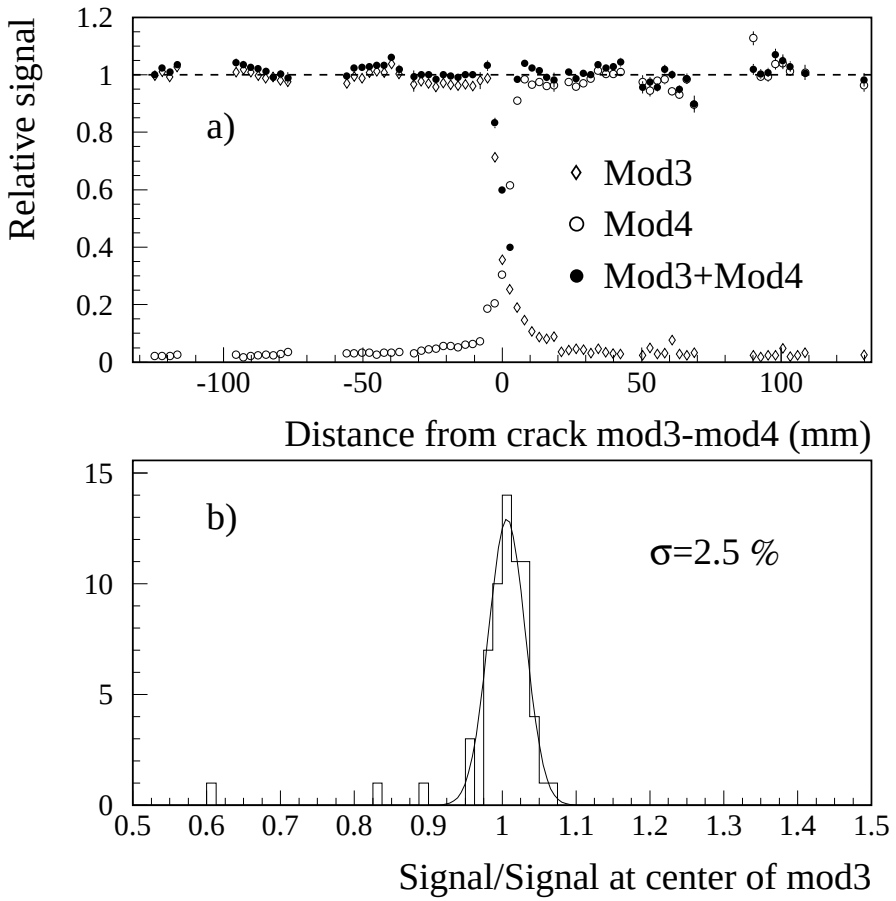

Figure 7: (a) Uniformity scan along the ϕ direction, obtained with 180 GeV muons impinging at $\theta = 10^o$. Plotted points represent the most probable value of the energy deposited. (b) The resultant normalized distribution of the most probable value of the energy deposited by muons. Experimental data is shown.

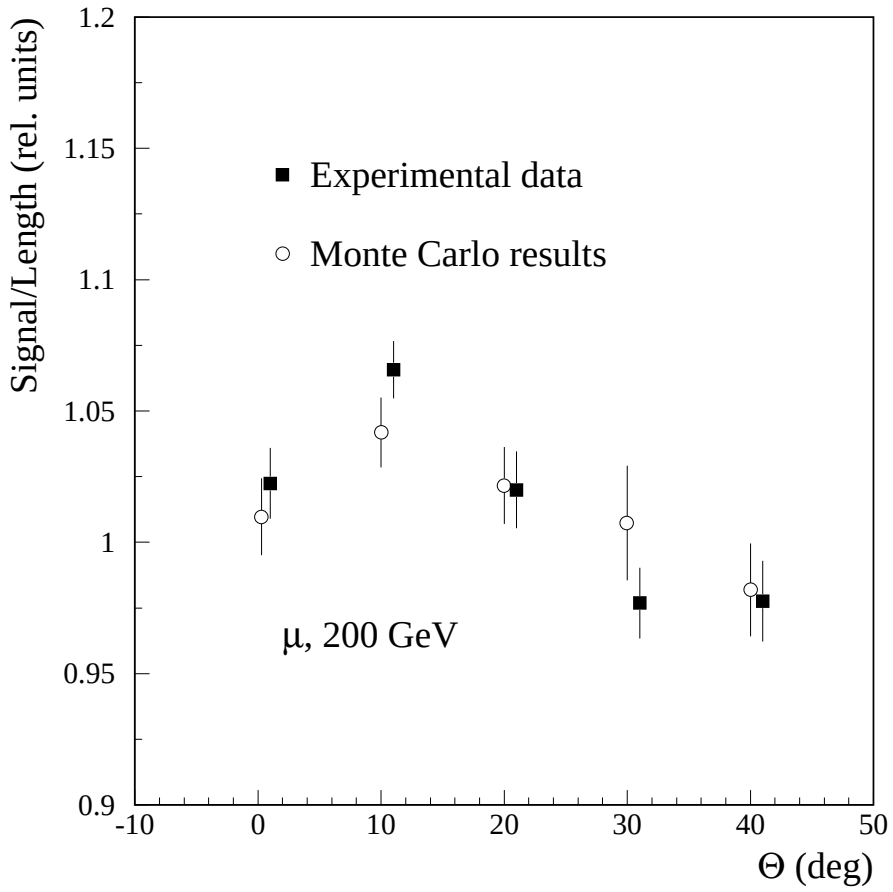

Figure 8: The average muon energy loss measured with the Tile calorimeter prototype normalized to the same path length as a function of the polar angle θ. Experimental data and MC simulations are shown.

Figure 9: Energy loss in the Tile calorimeter from simulation (MC) and experimental data for muons of 20 , 100 and 200 GeV traversing the full Tile calorimeter length (9 λ) at a polar angle of $\theta = 10^o$.

Figure 10: The truncated mean energy loss and the energy lost at the peak of the distribution (most probable value), for the Tile calorimeter as a function of the muon energy at a polar angle $\theta = 10^o$. The means are obtained ignoring data points above 5 σ_M. The experimental data (solid points) are compared to our simulation results (open points).

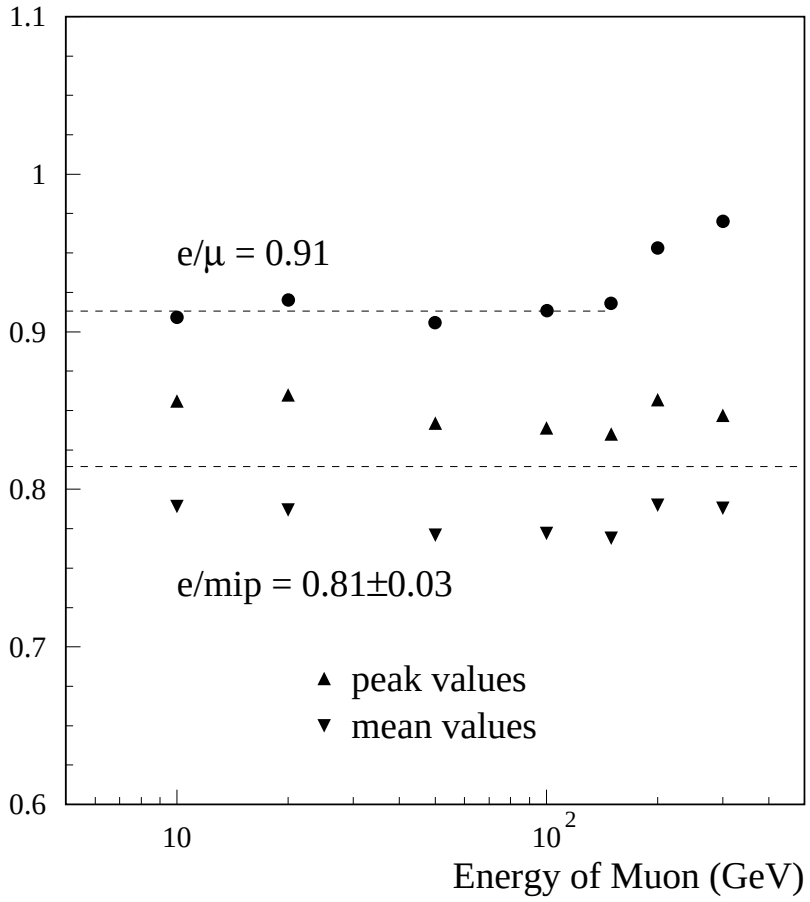

Figure 11: The e/mip ratio (triangles) and the e/μ ratio (dots) for the Tile calorimeter as a function of the muon energy and for a polar angle $\theta = 10^o$. The calculation of e/mip was performed for both the energy lost at the peak of the distribution (most probable value) and the mean value of the energy lost.

Figure 12: The simulated (MC) energy loss in the scintillator (in MeV) as a function of the energy lost in the Tile calorimeter absorber (in GeV) for 2, 10, 50 and 300 GeV incident muons. Here the energy deposited in each medium is given, without correcting for the respective sampling fraction and without normalizing to experimental data.

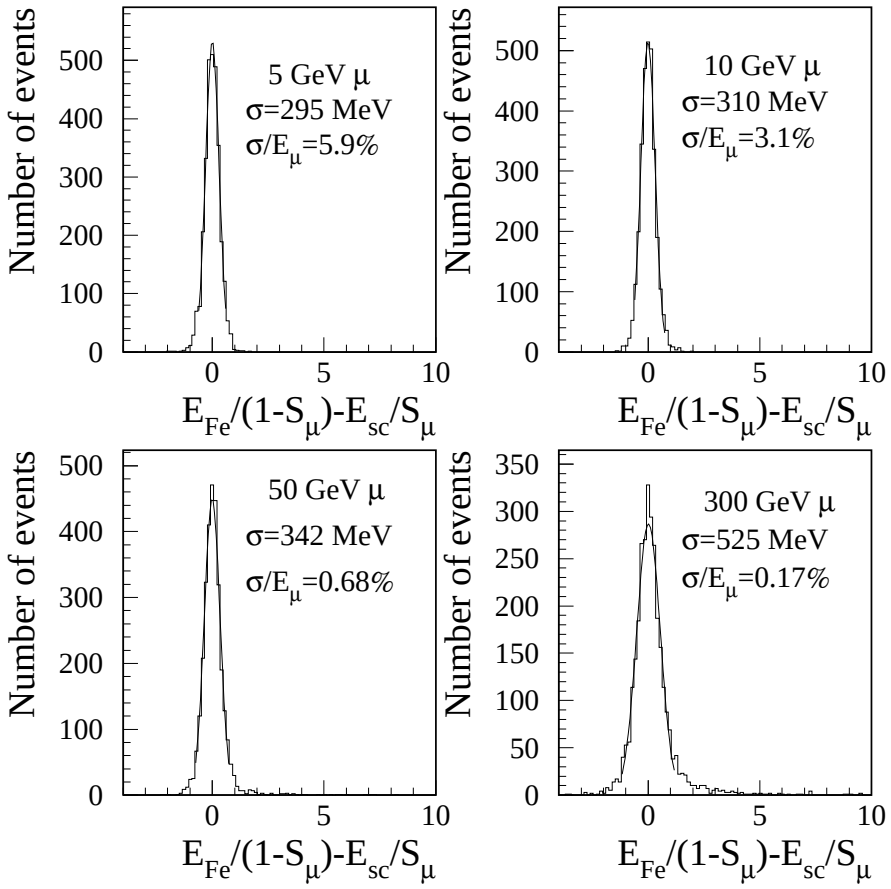

Figure 13: Simulation results showing the difference (in GeV) between the energy lost in the Tile calorimeter absorber, corrected for the sampling fraction in iron, and the energy lost in the scintillator, corrected for the sampling fraction in the scintillator.

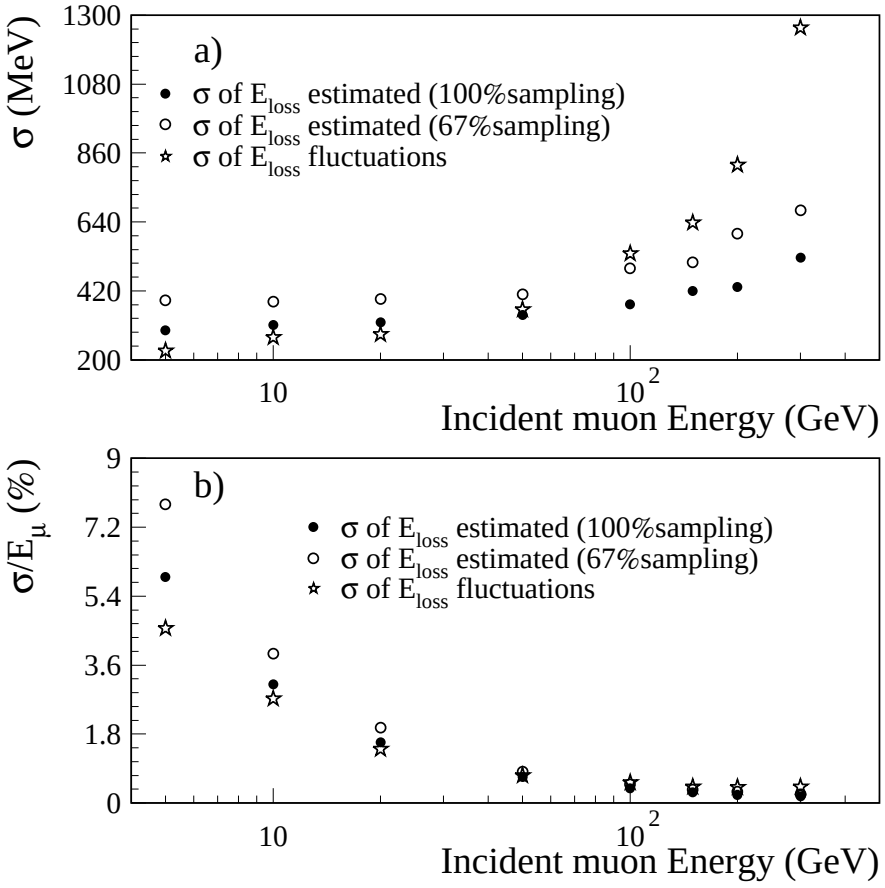

Figure 14: Spread of the MC difference distributions defined as in Fig. 13 vs. muon energy. The σ, obtained from a Gaussian fit within ± 2 σ, is given in (a) as MeV, and in (b) relative to the incident muon energy (σ/E_μ) The black dots show sampling over the full calorimeter depth of 80.5 X_0 and the open circles show sampling only over 67% of the active calorimeter depth. The stars represent the σ_M values for the Moyal fits to the energy loss spectra.

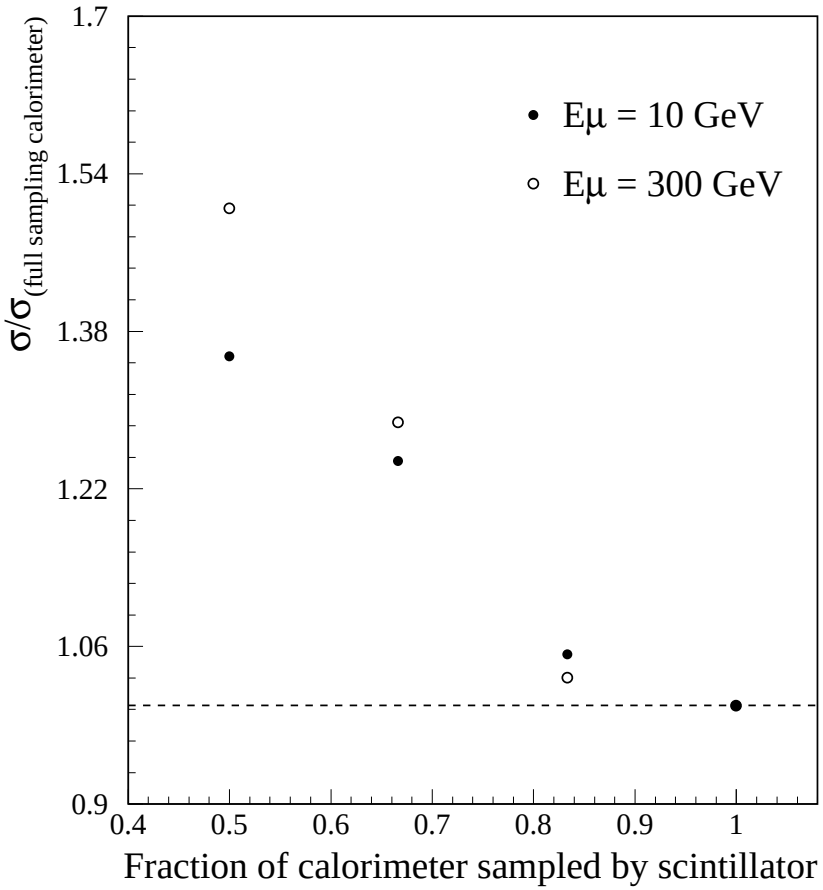

Figure 15: The relative resolution on the estimate of the energy loss in the prototype Tile calorimeter as a function of the fraction of the calorimeter which is sampled by the scintillator. The fractions shown are arrived at simply by adding the response of two or more contiguous depth samples. The resolution is shown for simulations of 10 and 300 GeV muons and is normalized to the resolution found with full calorimeter sampling (80.5 X_0).

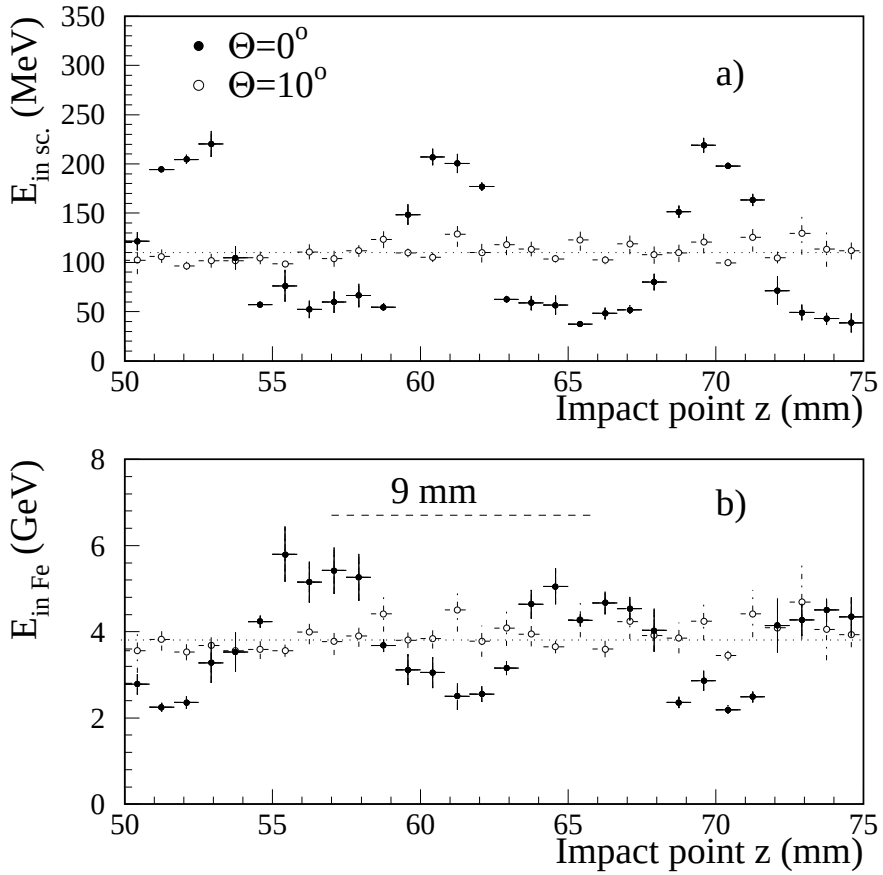

Figure 16: Simulation result showing the energy deposited in (a) the scintillator and (b) in the iron as a function of the Tile calorimeter z impact point for 180 GeV muons entering in the Tile calorimeter at $\theta = 0^o$ and $\theta = 10^o$.

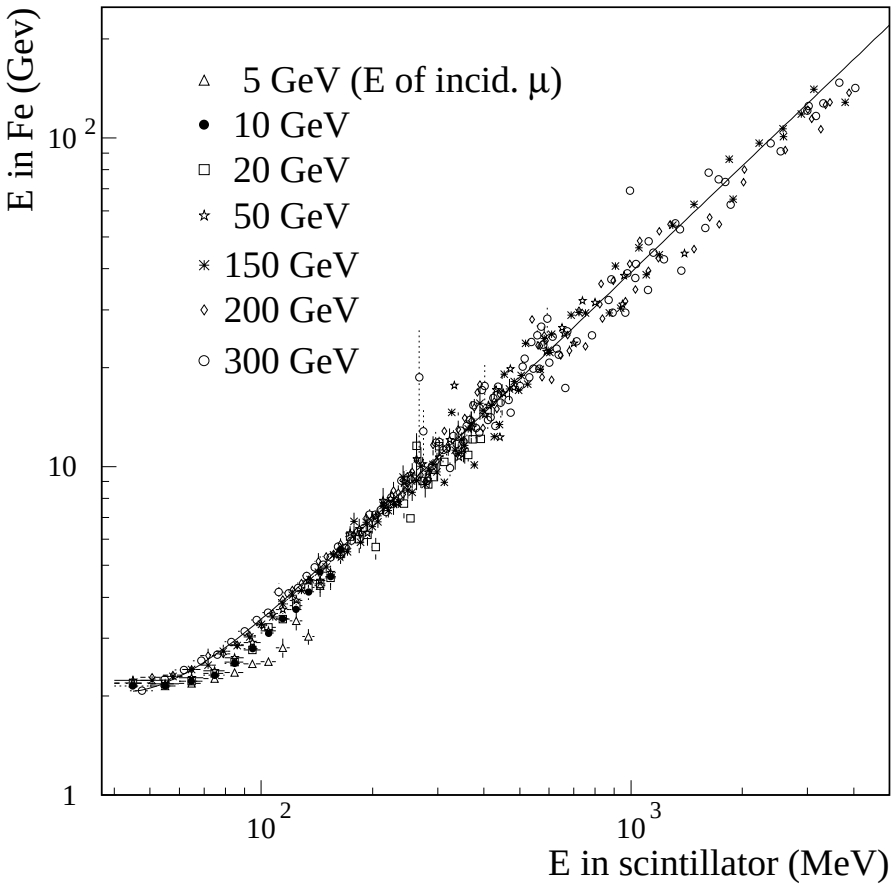

Figure 17: Simulation result showing the energy loss in the scintillator (in MeV) as a function of the energy loss in the Tile calorimeter absorber (in GeV) for incident muon energies between 5 and 300 GeV. The full curve is a parameterization to the data for 300 GeV muons.

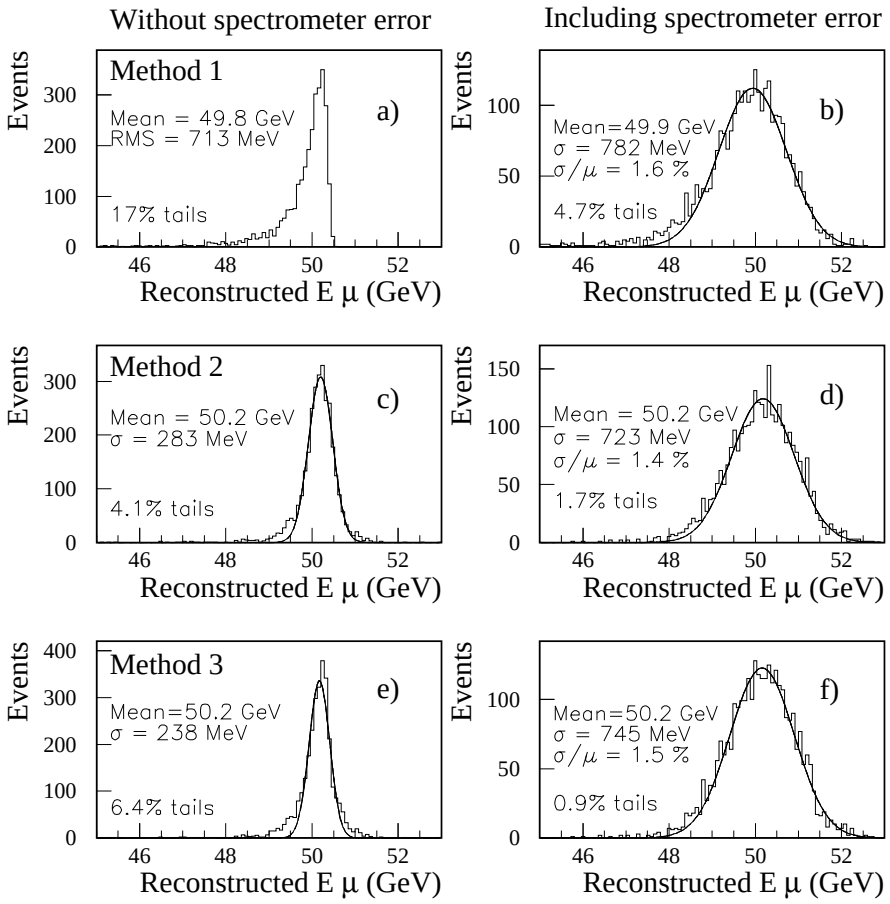

Figure 18: The expected energy distribution for 50 GeV muons after traversing the Tile calorimeter prototype using different methods to correct for the energy losses in the calorimeter. Method 1 adds to each event the most probable value of the energy lost in the calorimeter (2.40 GeV) (a) before smearing, (b) after smearing with the contribution from multiple scattering and the measurement/alignment error in the muon chambers. Method 2 corrects event by event, for the energy loss in the calorimeter (c) before smearing, (d) after smearing. Method 3 is a mixture of the first two methods using Method 1 for events with $E_{scintillator} \leq 80$ MeV and Method 2 for events with $E_{scintillator}$ above 80 MeV (e) before smearing, (f) after smearing.